Polym. Bull.
https://doi.org/10.1007/s00289-018-2356-4

ORIGINAL PAPER

Role of quaternary ammonium compound immobilized metallic graphene oxide in PMMA/PEG membrane for antibacterial, antifouling and selective gas permeability properties

Saz Muhammad[1,2] · Muhammad Siddiq[2] · Javed H. Niazi[1] · Anjum Qureshi[1]

Received: 31 January 2018 / Revised: 14 April 2018 / Accepted: 3 May 2018

Abstract Recently, there is a high demand for development of polymeric membrane for their widespread technological applications. Polymer blends incorporation with inorganic composite particles is the most effective strategy for obtaining antifouling, antibacterial, gas and water permeable membrane materials. However, their biological and surface properties are always hindered by the inefficient interaction of filler into polymer matrix because it is distributed into the bulk membrane matrix. In this study, graphene oxide nanosheets are incorporated with metal (Ag)/metal oxide (ZnO) composite filler (MGO) followed by surface modification with quaternary cetyltrimethylammonium bromide (CTAB) to enhance non-covalent interactions between filler and poly methyl methacrylate (PMMA)/polyethylene glycol (PEG) blend membrane. The membrane was utilized for improving antifouling, antibacterial and gas permeability of membrane. Our results indicated that CTAB-modified filler (CTAB@MGO) was bonded to the polymer blend membrane without affecting the membranes' physicochemical properties. The prepared CTAB@MGO–PMMA/PEG membrane showed excellent antibacterial property against model *Escherichia coli* bacteria. The antifouling activity and CTAB stability results of modified blend membrane ensured reduced bovine serum albumin adsorption and slow dissociation of surfactant molecules, respectively. The CTAB@MGO–PMMA/PEG blend membrane also showed promising gas permeability results with hydrogen (H_2), nitrogen (N_2) and carbon dioxide (CO_2). The presented approach highlights the potential of

Electronic supplementary material The online version of this article (https://doi.org/10.1007/s00289-018-2356-4) contains supplementary material, which is available to authorized users.

✉ Anjum Qureshi
anjum@sabanciuniv.edu

[1] Sabanci University SUNUM Nanotechnology Research Centre, Orta Mahalle, 34956 Tuzla, Istanbul, Turkey

[2] Department of Chemistry, Quaid-i-Azam University, Islamabad 45320, Pakistan

Published online: 08 May 2018

surface modification of filler and introduces them in polymeric membrane as a simple, easy and cost-effective strategy for preparing antifouling and gas/water permeable polymeric membranes.

Keywords Metallic graphene oxide · CTAB · Surface modification · Antifouling · Antibacterial · BSA adsorption · Gas permeability

Introduction

Recently, there is a high demand for development of polymeric membranes for their widespread biomedical and environmental applications, such as filter/water/gas permeable membrane, adsorption of contaminants, biomedical surgical tools, bioimplant materials, optical display, energy materials and food packaging [1–7]. One of the major issues that hinders performance and restricts the application of polymeric membranes is their fouling and nonspecific microbial adsorption (bacteria) [8, 9]. There have been few approaches employed to minimize the membrane fouling, which includes pre-chlorination of the feed solution [10], UV-induced grafting [11], surface modification/grafting [12, 13], incorporation of inorganic additives in polymer [14] and blending modifications [15, 16]. All the above-mentioned approaches are shown to be highly effective to improve the performance of the polymeric membranes. However, a few of the methods are energy consuming, require complex procedures and produce toxic by-products [17]. Among these, use of polymeric blend membrane incorporated with inorganic composite particles is the most economic and effective strategy to enhance the mechanical, thermal and antibacterial properties [18]. Additionally, inorganic composite particle in polymer blend membranes can improve water/gas permeability and selectivity in separation applications [19].

Therefore, synthesis of polymer blend hybrid membrane with tailored morphological, mechanical and physico-chemical characteristics is a robust approach and easy to scale up for efficient innovative applications. Despite many advantages, there are challenges to prepare blend membrane with inorganic additives, such as uniformity in physico-chemical properties and degradation of polymers through oxidation upon dispersion of additive and inorganic particle [20, 21]. Hydrophobic polymer, such as poly (methyl methacrylate) (PMMA) is easily miscible with poly (ethylene glycol) (PEG) domains (up to 30% PEG content). PEG has inherent pore-forming ability, hydrophilicity (polar nature) that plays a major role for its suitability in polymer blend membrane applications [1, 8]. PMMA/PEG blend membrane combinations have been demonstrated to exhibit excellent biocompatibility, gases permeability and selectivity due to van der Waals interactions between PMMA and PEG [8, 22]. Further, inorganic particles and their nanohybrids/composites, such as silver (Ag), zinc oxide (ZnO), graphene oxide are utilized for their antibacterial, antifouling, gas and water permeability applications [23–27].

Recently, surface modification of filler through either chemical grafting or physical adsorption is used to improve the interaction between filler (inorganic particles) and polymers, which resulted in a uniform dispersion of filler in polymer matrix

[28–30]. In physical modification, chemicals such as organic acids, surfactants are used to modify the surface properties of filler through electrostatic and van der Waals interactions between polar groups of the chemical and polymer moieties [29]. The use of surfactant-modified filler in polymers has several advantages, such as slow release of free surfactant molecules to minimize the toxicity in the environment and also prevent filler-induced degradation of polymer [31, 32]. CTAB is a ammonium-based compound and uses as a biocidal agent and plays a promising role in development of self-sterilized hybrid polymer membrane [31, 33, 34]. However, use of nanohybrid combination of organic–inorganic fillers, such as graphene oxide and metal/metal oxide into polymer, has not yet been explored. Use of such polymers has the potential for synthesizing antibiofouling membranes using a robust and environmentally friendly alternative method for gas/water permeability and other environmental- and biomedical-related applications.

Therefore, in this work, surface modification of graphene oxide with metal (Ag)/metal oxide (ZnO) filler combination (MGO) was carried out using CTAB and dispersed metallic Ag/ZnO-reduced graphene oxide (MGO) into PMMA/PEG blend membrane. The effect of CTAB-modified MG in PMMA/PEG blend membrane (CTAB@MGO blend) was studied with respect to their structural and thermal properties. The biological properties, such as antibacterial and antifouling activity of CTAB@MGO-PMMA/PEG membrane were studied against *Escherichia coli* strain as a model microorganism. The gas permeability of CTAB@MGO blend membrane was tested with H_2, N_2 and CO_2 gases.

Materials and methods

Materials

All chemicals used in this study were of analytical grade and used without further purification. Poly methyl methacrylate (PMMA, M_w 350,000 g/mol) and poly ethylene glycol (PEG Bio Ultra, 4000 M_w 3500–4500 g/mol), silver nitrate (99.00% purity), cetyltrimethylammonium bromide (CTAB), ammonium hydroxide and bovine serum albumin (BSA) were obtained from Sigma-Aldrich, Germany. Dimethyl sulfoxide (DMSO) was procured from AppliChem, and zinc acetate dehydrate was obtained from Merck, Germany. Luria-Bertani broth (LB-broth) and Luria-Bertani agar (LB-agar) were obtained from Difco (MI, USA). Wild-type *E. coli* DH5α strain was used as model bacterial cells for antifouling and antibacterial study.

Synthesis of metallic Ag/ZnO-reduced graphene oxide (MGO)

Graphene oxide (GO) gel was prepared by suspending 30 ml of 1 mg/ml GO sealed in a 50 ml Teflon-lined autoclave chamber placed in an oven at 180 °C for 6 h. The autoclave was allowed to cool down to room temperature. In a separate reaction, 45 ml of 0.168 M $AgNO_3$ and 90 ml of 1 M $Zn(COOCH_3)_2$ solutions were mixed. The resulting mixture was further added with appropriate amount of ammonium hydroxide solution (28 wt%) under vigorous stirring until a clear solution of

coordination compound of ($[Zn(NH_3)_4]^{2+}$/$[Ag(NH_3)_2]^{+}$) appeared in the reaction mixture. The GO gel was then suspended in 40 ml of ($[Zn(NH_3)_4]^{2+}$/$[Ag(NH_3)_2]^{+}$) solution, and the mixture was heated to 70 °C under vigorously stirring for 1 h. Thus obtained metallic GO gel was heated in a furnace at 750 °C for 2 h in inert atmosphere for the thermal annealing. The detailed synthesis procedure is as illustrated in Scheme 1. As-synthesized metallic Ag/ZnO-reduced graphene oxide (MGO) was later subjected to characterization by scanning electron microscopy (SEM, Leo Supra 35VP), XRD and Raman spectroscopy (Renishaw in Via Reflex Raman microscopy with a laser of 532 nm in the range 450–3000 cm^{-1}).

Immobilization of CTAB on MGO

For the immobilization of CTAB on MGO, a mass ratio of 8:1 (CTAB:MGO) was mixed in DI water and subjected to sonication for 30 min under continuous stirring. The resulting mixture obtained was washed thrice with DI water and dried at room temperature. CTAB-immobilized MGO (CTAB@MGO) was later characterized by SEM, Fourier transform infrared spectroscopy (FTIR Thermo scientific Nicolet™ iS™10), zeta potential (Malvern instruments, UK) and Thermogravimetric analyzer (TGA, Netzsch STA 449 C, Germany) analysis.

Preparation of blend membrane

Four different combination of polymeric blend membranes, such as PMMA/PEG neat, PMMA/PEG/CTAB (CTAB blend), PMMA/PEG/MGO (MGO blend) and PMMA/PEG/CTAB@MGO membranes were prepared by solution casting method. The detailed composition of each blend membrane is given in Table S1 (SI). Briefly, first PMMA/PEG (12 g/4 g) was dissolved in DMSO (84 g) under continuous stirring and obtained the homogeneous blend solution. Secondly, a pre-weighed amount

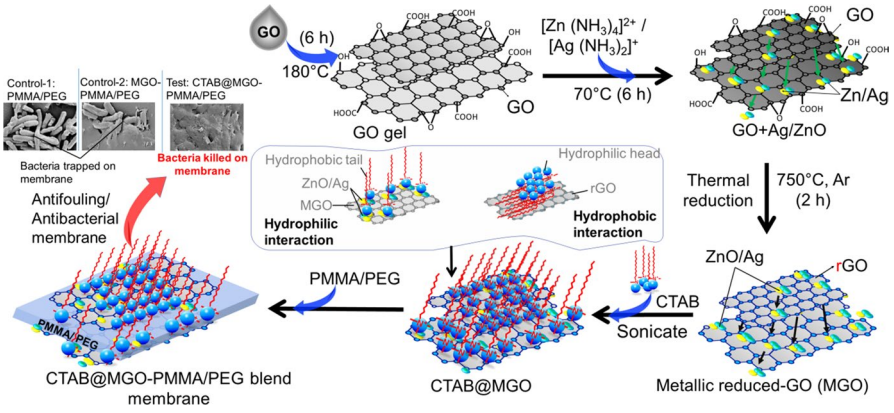

Scheme 1 Schematic diagram showing sequential reaction steps during the synthesis of metallic Ag/ZnO-reduced graphene oxide (MGO) membrane that is designed for its application in antifouling/antibacterial properties

of MGO and CTAB@MGO was uniformly dispersed in DMSO through sonication and further mixed with polymer blend solution under continuous stirring at 60 °C for 12 h followed by degassing in a desiccator, respectively. The solutions were casted in petri dishes, separately, and solvent was evaporated at 40 °C under standard conditions. Further, neat PMMA/PEG and CTAB blend membranes were prepared separately using above-mentioned procedures and considered as control membranes.

Blend membrane characterizations

Thermal stability of blend membranes were analyzed by TGA analyzer (Netzsch STA 449 C thermo-microbalance with TG resolution of 0.1 μg) at 10 °C/min in air (flow rate 30 ml/min) from 25 to 600 °C. Differential scanning calorimetry (DSC-Q2000 TA instruments, USA) characterization was performed from −50 to 200 °C at 10 °C/min under nitrogen flow (rate 50 ml/min). The surface morphology of the membrane was studied by optical micrographs (Carl Zeisis microscope) and SEM (Leo Supra 35VP) analysis. The samples were coated with gold metal at a voltage of 0.04 V/Ω using Cressington sputter coater 108/SE before SEM imaging. FTIR and Raman spectra of membrane samples were recorded using Nicolet iS10 FTIR spectrometer (600–4000 cm^{-1} with 4 cm^{-1} resolution) and Renishaw in Via Reflex spectrometer (laser wavelength 532 nm with 5 cm^{-1} spectral resolution), respectively.

Antibacterial activity of blend membranes

The antibacterial activity of the blend membrane samples was measured against *E. coli* DH5α strain by measuring their growth and cell viability. For this, fresh cells were cultured in a LB-broth at 37 °C and harvested by centrifugation at 10000 rpm for 1 min. The cells were washed thrice with PBS (phosphate buffer saline, $M = 0.01$, pH = 7.4) to ensure removal of all nutrients from the broth. The cells were re-suspended in PBS and the cell concentration adjusted to an approximate 10^8 cells/ml. Blend membranes used for antibacterial studies were first washed with de-ionized water to remove loosely bound precursors and dried at 50 °C in a vacuum oven. The clean blend membranes were subjected to UV sterilization for 25 min. The specific size of membrane coupons (active surface area = 0.5 cm^2) were cut out from each blend membrane samples in replicates for antibacterial studies. These control and test blend membrane coupons were placed in wells of 96-well microtitre cell culture plates in replicates ($n = 3$). Bacterial cell suspension (10^8 cells/ml) was then inoculated across the 96-well cell culture plates that had a transparent bottom (BRANDplates®) allowing to measure the absorbance spectrophotometrically. The cell culture plate was then incubated at 37 °C, and the growth of the cells was recorded every 10 min interval for 10 h at 600 nm using Synergy HTX multimode microplate reader (Biotek).

Further, agar plate experiment was conducted to measure the antibacterial effect of blend membrane samples on *E. coli*. Briefly, each type of membrane coupons with 6 mm diameter was placed into Luria-Bertani (LB) broth and incubated at 37 °C for 12 h. Here, the blend membranes were overlayed on an LB-agar surface unlike suspension in liquid medium and incubated with *E. coli* culture

solution. The cleared zones formed around the disks were measured manually for antibacterial activities of the membrane coupons.

Antifouling studies of blend membranes

For the antifouling experiment, bacterial culture and dilution was prepared using the same method as described for antibacterial studies. SEM imaging was performed to understand the antifouling effect of bacterial cells' attachment on CTAB@MGO blend membrane and control blend membrane samples. For this, membrane coupons with 1-cm^2 area were cut from already washed, rinsed and sterilized blend membrane samples. These coupons were immersed in PBS containing 10^8 cells/ml bacterial suspension and incubated on a rotary shaker at 37 °C for 12 h. Membrane coupons were fixed prior to SEM imaging using 1% (v/v) glutaraldehyde solution at 4 °C for 30 min, followed by subjecting to ethanol dehydration steps with 30, 50 and 90% ethanol, respectively, and dried at room temperature.

Antifouling studies of blend membrane were also carried out by testing the adsorption of protein on blend membrane samples. For this, membrane coupons with 6 mm diameter were cut and washed thoroughly with PBS several times. The membrane coupons were transferred to 1 ml of BSA solution (1 g/l in 0.5 M PBS), and the solution was shaken at 25 °C for 8 h with shaking rate 120 rpm. The BSA solution without membrane coupon was also kept under identical conditions which is considered as a control. The concentration of BSA before and after adsorption with membrane coupon samples was determined by measuring the optical density of solution at 280 nm using Synergy HTX multimode microplate reader (Biotek).

Gas permeability measurement of blend membranes

The permeability of hydrogen (H_2), nitrogen (N_2), and carbon dioxide (CO_2) was carried out with blend membrane samples in the pressure range between 8 and 10 psi at room temperature. The Fick's formula was used to calculate the permeability of gases as shown in Eq. 1:

$$P = \frac{K \times d \times s}{\Delta p \times t} \tag{1}$$

where K is cell constant, d is the thickness of the blend membranes, s is displacement of mercury (Hg) slug in U-tube of gas permeability setup, Δp is pressure gradient and t is the time taken in displacement of Hg slug level. The unit of gas permeability is expressed in barrer (1 barrer = 10^{-10} cm^3 (STP) cm/cm^2 s cm-Hg). Membrane blends were stabilized for at least 1 h at 10 psi and triplicate measurements were taken for statistical analysis. The detailed schematic diagram of gas permeability setup is given elsewhere [35].

Results and discussion

Characterization of MGO

Metallic Ag/ZnO-reduced graphene oxide (MGO) was prepared by hydrothermal method. Raman spectrum of control GO and MGO (test) is shown in Fig. 1a. The absence of defects band (D-band) in Raman spectra of MGO as compared with GO confirmed the deposition of Ag/ZnO heterostructures over reduced graphene oxide (rGO) layer with negligible defects in graphene nanostructure, which is consistent to a previous report [36]. SEM images confirmed the presence of bi-metallic Ag/ZnO heterostructures decorated on rGO sheets in MGO (inset Fig. 1a). The phase structure of MGO was analyzed by XRD, and the XRD peaks corresponding to Ag, ZnO and rGO in MGO were observed (Fig. 1b). The XRD profiles of as-synthesized MGO indicated the presence of Ag with peak (111), (200) and (220) (JCPDS reference code 01-087-0717), and ZnO peaks were observed at (002), (101) and (004) (JCPDS reference code 79-0208) were consistent with earlier reports on bi-metallic nanostructures [37]. The shoulder hump around at $\theta \approx 25^{\circ}$ was assign to the rGO structure.

Immobilization of CTAB on MGO

The CTAB immobilization on MGO resulted in a rugged paper of graphene like structure on MGO giving rise to a characteristic morphology of CTAB@MGO structure (Fig. 2a). The surface modification of MGO with CTAB was further analyzed by FTIR (Fig. 2b) and the FTIR spectra of CTAB@MGO showed characteristics peaks of both MGO hybrid and CTAB molecules that includes stretching vibration and C–H bending vibration (1470 cm^{-1}), C=O stretch (1635 cm^{-1}), secondary N–H group stretching (3014 cm^{-1}), CH_2 symmetric and antisymmetric

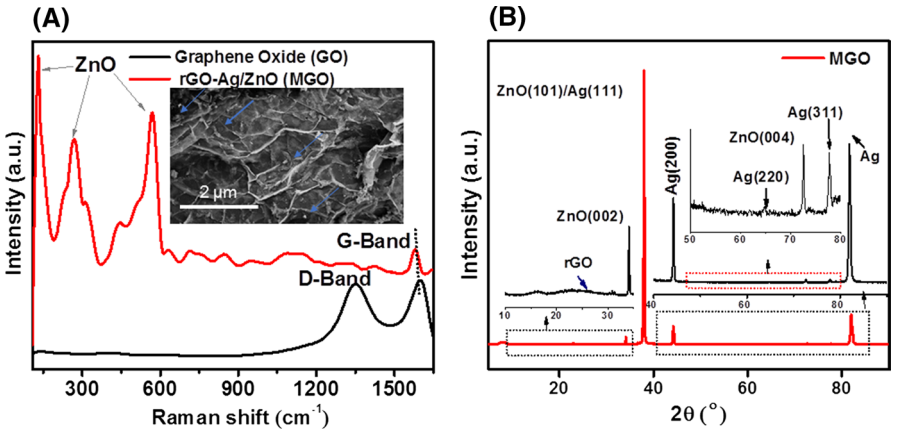

Fig. 1 **a** Raman spectra of MGO sample and SEM image shown in the inset and **b** XRD spectra of MGO and the inset figures are the expanded regions derived from the main XRD spectrum

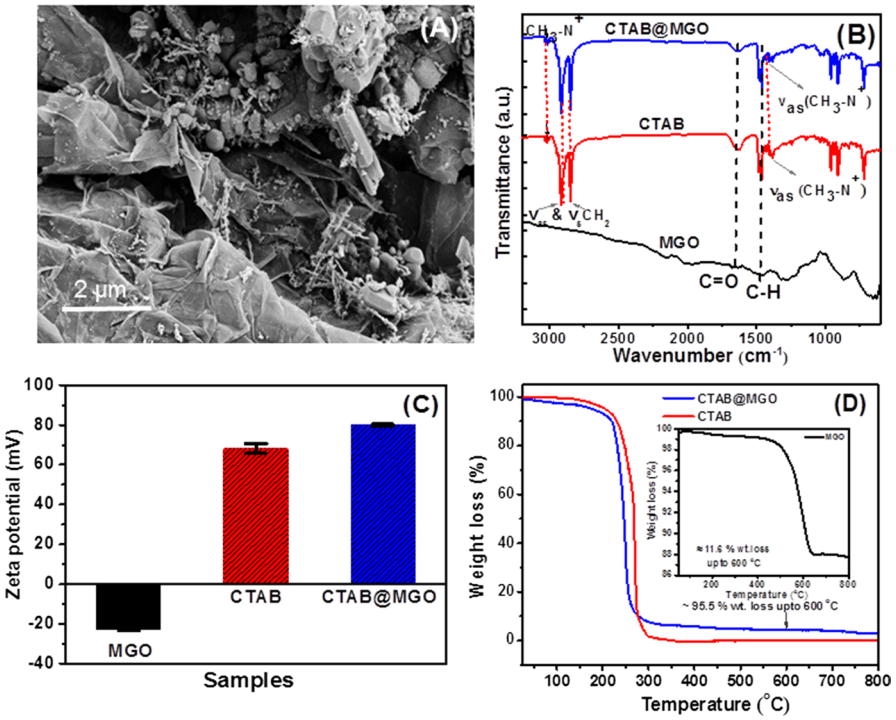

Fig. 2 **a** SEM image of CTAB@MGO, **b** FTIR spectra, **c** zeta potential (≈pH 7.6) and **d** TGA curves of CTAB and CTAB@MGO samples with TGA curve for MGO shown separately in the **d** inset figure

vibrations (2915 and 2850 cm^{-1}) and C–H asymmetric scissoring vibrations of CH_3–N^+ groups of CTAB (1415 cm^{-1}) [30, 38]. It suggested physical modification/stacking of MGO through electrostatic interaction between positively charged quaternary ammonium groups of CTAB and negatively charged rGO decorated with metals.

Zeta potential measurements were made with surface modified MGO with CTAB (CTAB@MGO) at pH of 7.6. Zeta potential values of -23.1 ± 0.7 mV with pristine MGO structure drastically shifted to 80 ± 0.45 mV after CTAB immobilization (Fig. 2c). This shift is attributed to the positively charged quaternary ammonium groups in the CTAB compound (zeta potential value 68.16 ± 2.45 mV), suggesting successful immobilization of CTAB on metallic graphene carriers.

The component ratio of CTAB in CTAB@MGO hybrid was analyzed by measuring weight loss by TGA analysis of MGO, CTAB and CTAB@MGO from 20 to 800 °C, respectively (Fig. 2d). The weight loss of CTAB@MGO and MGO was recorded to be ~95.5% (Fig. 2d) and 11.5% (Fig. 2d inset), respectively with maximum up to 600 °C. Therefore, the differential weight loss among CTAB@MGO and MGO was found to be 84% which corresponds to CTAB and verified with the theoretical ratio of CTAB to MGO in CTAB@MGO. Since the CTAB@MGO was prepared by taking their mass ratio (8:1), therefore respective weight% was calculated from their TGA thermograms to check their theoretical ratios. Based on two weight

losses, the ratio of CTAB and MGO was calculated to be ≈7.3, which were almost consistent with the theoretical value of 8.

Blend membranes and their physicochemical properties

In this study, synthesized CTAB@MGO hybrid was exploited as a biocide and inhibitor for PEG susceptibility in PMMA/PEG blend membrane. This membrane was designed to acquire fouling resistance, antibacterial activity, and permeability applications. Four different combinations of polymeric blend membranes were prepared in order to study the effect of immobilization of CTAB on physicochemical properties of PMMA/PEG blends. These include PMMA/PEG neat blend, CTAB/PMMA/PEG (CTAB blend), PMMA/PEG/MGO (MGO blend) and PMMA/PEG/CTAB@MGO membranes.

It is clear from TGA curves that CTAB@MGO incorporation in blend showed stable thermal behavior as compared with MGO blend (Fig. 3a). This result suggested that CTAB immobilization improved thermal stability of blend membrane. This is attributed to the intercalation of CTAB and MGO that promoted the dispersion/interactions of CTAB@MGO with the blend and provided susceptibility to polymeric blend against metal-induced oxidation [31, 39]. TGA curves of each blend membrane exhibited weight loss in two stages at ~220 and ~370 °C which account for the two major components of PEG and PMMA in blend membranes, respectively (Fig. 3a inset). The starting degradation temperature was found to be ~195, 180 and 190 °C for CTAB, MGO and CTAB@MGO blend membrane, respectively (Fig. 3a). Also, CTAB@MGO blend membrane exhibited moderate increase in thermal stability with second stage maximum weight loss at around 372 °C as compared to 368 °C with MGO blend membrane according to TGA derivative plots (Fig. 3a inset). This is attributed to the role of CTAB as inhibitor for PEG and restricting the affinity of PEG with MGO in CTAB@MGO blend [31, 40].

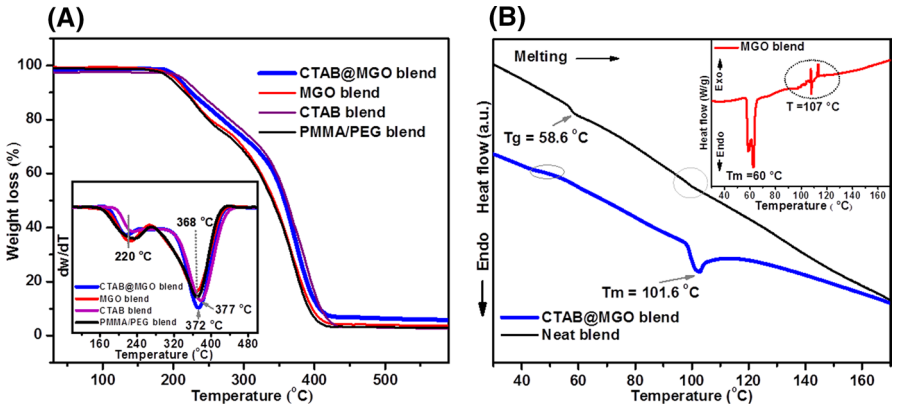

Fig. 3 **a** Thermogravimetric analysis (TGA) and the inset figure shows the first derivative of % weight loss in TGA under air. **b** Differential scanning calorimetric (DSC) curves of neat, and MGO@CTAB blends and the inset figure shows DSC curve of MGO blend under nitrogen flow

The DSC profile of PMMA/PEG neat, MGO and CTAB@MGO blend membrane were shown in Fig. 3b. The DSC curve of neat blend showed two glass transition temperatures at T_g ~ 58.6 and ~ 100 °C with respect to PEG and PMMA, respectively (Fig. 3b). The presence of peak at ~ 60 °C is related to melting of MGO blend (Fig. 3b inset) and hysteresis effect of MGO in polymer blend was observed at 107 °C. These results suggested that MGO incorporation in polymer blend was not completely miscible as observed with irregular coarser spherulites from their optical images (Fig. 4c). The glass transition and melting temperature for CTAB@MGO blend membrane were observed at ~ 57 °C and ~ 101.6, respectively. These results indicated that CTAB immobilization on MGO facilitated better compatibility with PMMA/PEG in CTAB@MGO blend membrane.

PMMA/PEG blend membranes were miscible due to PMMA carbonyl groups interactions with terminal OH of the PEG, represented by the formation of –C=O···H–O species. FTIR spectra were recorded to demonstrate such type of interactions

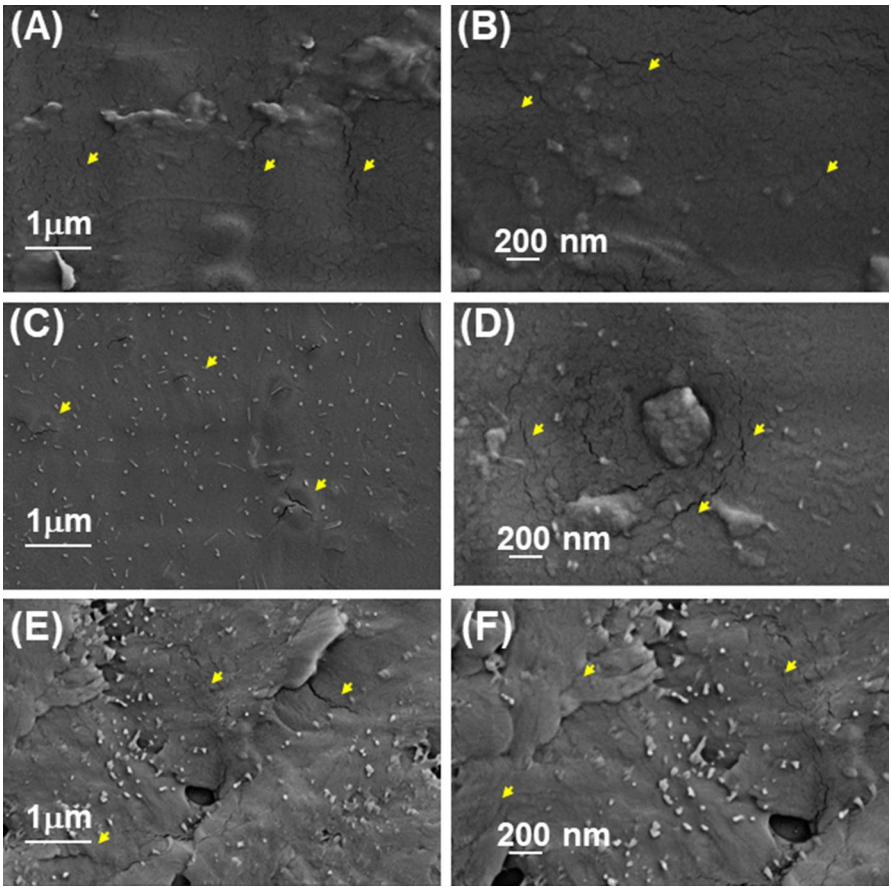

Fig. 4 Scanning electron microscope images of; **a**, **b** neat, **c**, **d** MGO and **e**, **f** CTAB@MGO blend membranes

and confirm the presence of these chemical moieties. FTIR spectra of the neat blend, CTAB blend, MGO blend and CTAB@MGO blend shown in Fig. S1A. FTIR spectra of neat blend showed two regions of 3100–2700 and 1800–1600 cm^{-1} that are arising due to PMMA/PEG interactions (Fig. S1A). Stretching vibrations at 2885 and 2955 cm^{-1} could be assigned to antisymmetric stretching vibration of CH_2 group of PEG and PMMA, respectively and stretching at 1723 cm^{-1} is assign to vibration of C=O group of PMMA [41].

These featured vibration stretching modes of PMMA and PEG were clearly appeared in the FTIR spectra of CTAB blend, MGO blend and CTAB@MGO blend. The stretching vibrations of secondary N–H group stretching (3018 cm^{-1}), CH_2 symmetric and antisymmetric vibrations (2915 and 2850 cm^{-1}) and C–H asymmetric scissoring vibrations of CH_3–N^+ groups of CTAB (1415 cm^{-1}) have appeared in the FTIR spectra of CTAB blend and CTAB@MGO blend [30]. It was observed that both CH_2 stretching vibrations (2915–2955 cm^{-1}) of PEG and CTAB groups were overlapping in the FTIR spectra of CTAB@MGO blend. Further, the intensity of C=O groups of CTAB@MGO blend tend to decrease which is accompanied by the appearance of CTAB functional groups when compared with intensity of C=O groups in control MGO blend. This result suggests the interaction between hydrophilic and hydrophobic components facilitated miscibility in the CTAB@MGO blend which is consistent with the DSC analysis (Fig. 3b). Raman spectra of neat PMMA/PEG blend, CTAB blend, MGO blend and CTAB@MGO blend were recorded as shown in Fig. S1B. The Raman spectra of CTAB@MGO blend clearly showed the characteristic G and 2D bands of rGO at 1585 and 2725 cm^{-1} as well as C–H, CH_3, O–CH_3 stretching at (1460 cm^{-1}) and C=O (1730 cm^{-1}) groups of PMMA and PEG [42, 43]. These results confirmed CTAB@MGO heterostructure is successfully incorporated in polymeric blend.

Optical microscopic images were taken to get more insight into the surface morphology of the prepared blend membranes as shown in Fig. S2A-D. The optical images clearly indicated the miscibility features of CTAB@MGO in PMMA/PEG blend as compared with MGO blend membrane (Fig. S2C-D), and this result is further supported by the results of TGA/DSC analysis with same membranes (Fig. 3a, b). The inter-lamellar regions and spherulites appearance in case of MGO blend membrane is more irregular and coarser as compared with CTAB@MGO blend membrane. The miscibility change and randomness in lamellar bundles observed in case of MGO blend membrane may be attributed to MGO-driven crystallization due to its heteronucleating particle nature [14].

The SEM images of PMMA/PEG neat blend membrane showed uniform miscibility without phase separation which is attributed to interactions of the oxygen of PEG with carbonyl carbon of PMMA (Fig. 4a, b). The phase separated domain of polymer components and irregular coarser morphology was observed on MGO blend membrane surface (Fig. 4c, d and Fig. S3C). This is due to distinctly different hydrophilic–hydrophilic interactions between MGO and PEG as compared with its interaction with PMMA component (hydrophilic–hydrophobic interaction) [44]. CTAB@MGO blend membrane surface clearly showed thick-layer morphology with small diffused crack networks (indicated with arrow) as compared with MGO blend (Fig. 4e, f). It is clear that immobilization of CTAB on MGO facilitated

hydrophilic–hydrophobic interactions between constituents of CTAB@MGO blend membrane, accompanied by reduction in solvent evaporation rate caused by CTAB during casting of blend membrane [30]. These results were also confirmed by their FTIR and Raman spectra (Fig. S1A-B).

Applications of CTAB@MGO blend membrane

In this study, CTAB@MGO blend membrane was subjected to further analysis for its antibacterial, antifouling and gas permeability properties.

Antibacterial and antifouling properties of the CTAB@MGO blend membrane

Antibacterial and antifouling performance of the modified membrane was determined using *E. coli* bacterium. The bacterial cells grown in growth medium amended with membrane samples and the growth of bacteria was measured from 0 to 10 h of incubation with membrane samples (Fig. 5a). The results showed that growth of cells was moderately reduced with neat blend (PMMA/PEG, control-1) and in the absence of membrane sample (control-2) (Fig. 5a). However, bacteria grown in the presence of CTAB@MGO blend membrane showed drastic reduction in cell growth as compared with control-1 and control-2 (Fig. 5a). These findings suggest that the metallic graphene oxide hybrid carrier exhibits moderate inhibition of *E. coli* cell growth activity, whereas the CTAB@MGO blended membrane demonstrated an excellent antibacterial activity (Fig. 5a).

Further, agar plate experiment was conducted to measure the antibacterial effect of CTAB@MGO membrane coupon against *E. coli* cells. Here, the blend membranes was overlayed on an LB-agar surface unlike suspension in liquid medium and incubated with *E. coli* culture solution. The resulting growth inhibition zones in the presence of control and test membranes were measured. It is clear from Fig. 5b that maximum antibacterial activity was found with CTAB@MGO blend followed by CTAB blend and MGO blend. Comparison of antibacterial activity among membranes revealed that CTAB@MGO exhibited 2.5-folds antibacterial activity as compared with antibacterial activity of MGO blend.

The bacterial growth patterns were consistent with bacterial adhesions as observed in SEM images (Fig. 5c–e). It is clear from the SEM examination that membrane without MGO (neat blend, Fig. 5c) showed relatively more adhesion of bacteria as compared to membrane with MGO and CTAB@MGO (Fig. 5d, e) blend membranes. The MGO blend membrane showed relatively less bacterial adhesion as compared with that observed with neat blend, and this clearly suggests the antibacterial and antifouling ability of Ag and ZnO on graphene surfaces in MGO blend membrane [14]. It is well known that most bacterial cell walls are negatively charged and have affinity for positively charged polymer system with quaternary ammonium groups as biocides [4]. SEM images of MGO@CTAB blend clearly showed maximum antibacterial/antifouling effects when compared with neat, CTAB and MGO blend membranes following their incubation with bacterial culture for 12 h (Fig. S4 and Fig. 5c–e). The antibacterial activity studies with membranes clearly

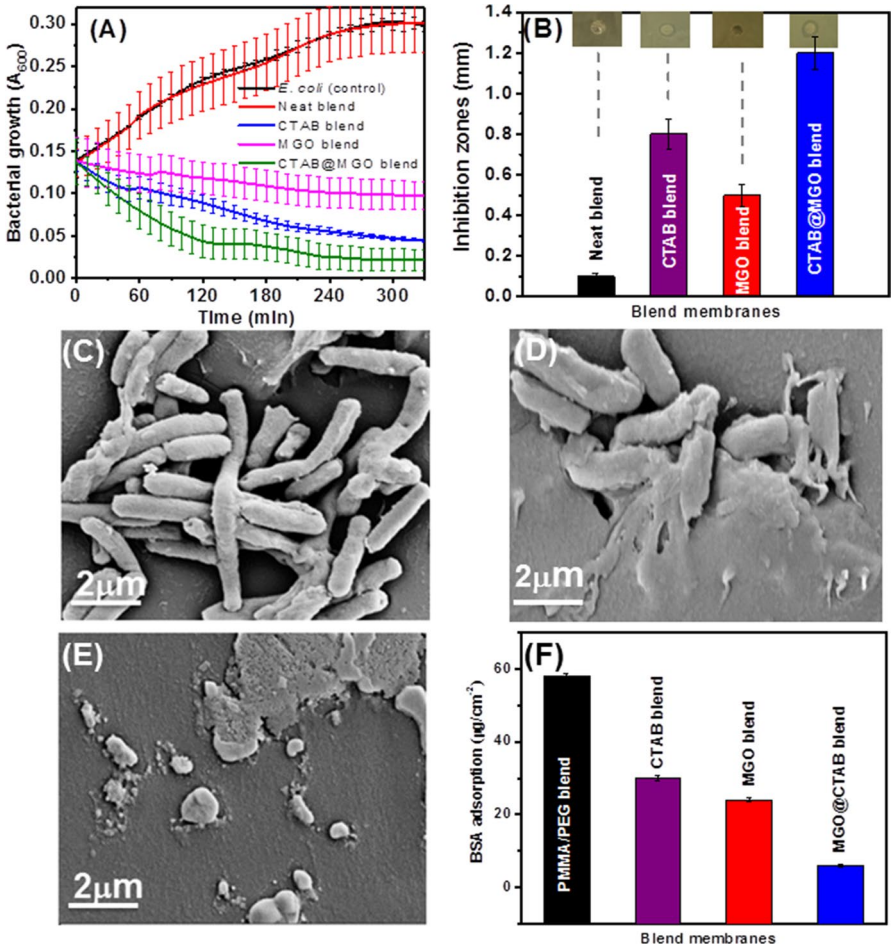

Fig. 5 **a** Growth curves of *E. coli* cells in LB-broth/agar medium amended with membrane samples including no membrane (NM) as control. **b** Inhibitory assay and antibacterial zone measurements against neat blend, CTAB blend, MGO blend and CTAB@MGO blend membranes. The inset figure shows images of plates with respective inhibitory zones on LB-agar plates. SEM images of blend membranes following exposure with *E. coli* for 12 h, such as; **c** neat (control) showing extensive adhesion of bacteria, **d** MGO blend membrane with relatively less bacterial adhesion, **e** CTAB@MGO blend membrane with partial adhesion of killed bacteria and **f** BSA protein adsorption measurement with all membrane coupon samples

demonstrated the CTAB immobilization on MGO providing efficient antibacterial activity against *E. coli* cells, which is attributed to the presence of CTAB as a carrier that minimize metal-induced degradation of polymer blend membrane and surface roughness of graphene layers.

Antifouling performance of blend membrane samples were determined by measuring the extent of adsorption of BSA protein on membrane coupon samples as described in experimental section. The BSA adsorption behavior with each

membrane coupon sample is shown in Fig. 5f. CTAB blend membrane exhibited less adsorption as compared with neat blend. MGO@CTAB membrane showed minimum adsorption of BSA protein as compared with other control blend membranes (Fig. 5f). Possible mechanism for minimum adsorption of protein on MGO@CTAB blend membrane could be explained due to presence of hydrophilic moieties of PEG, MGO and CTAB@MGO on the membrane (Scheme 2). The interaction between hydrophilic and hydrophobic components in blend membrane is evident from DSC, FTIR and Raman spectra. Therefore, the presence of these moieties in CTAB@MGO blend may seem to weaken the interactions of protein molecules and result in minimum protein adsorption.

Gas permeability of CTAB@MGO blend membrane

The physicochemical characterization of CTAB@MGO blend membrane showed excellent features, such as diffused small crack networks and uniform distributed CTAB-immobilized MGO in CTAB@MGO blend membrane, and therefore, this blend membrane was exploited for gas separation application. The gas permeation performance of blend membrane samples were carried out for H_2, N_2, and CO_2 gases, and related results are shown in Fig. 6 and Tables S2-S3. All of polymeric blend samples such as neat, CTAB, MGO and CTAB@MGO blend showed highest permeability for H_2 gas due to smaller molecular diameter

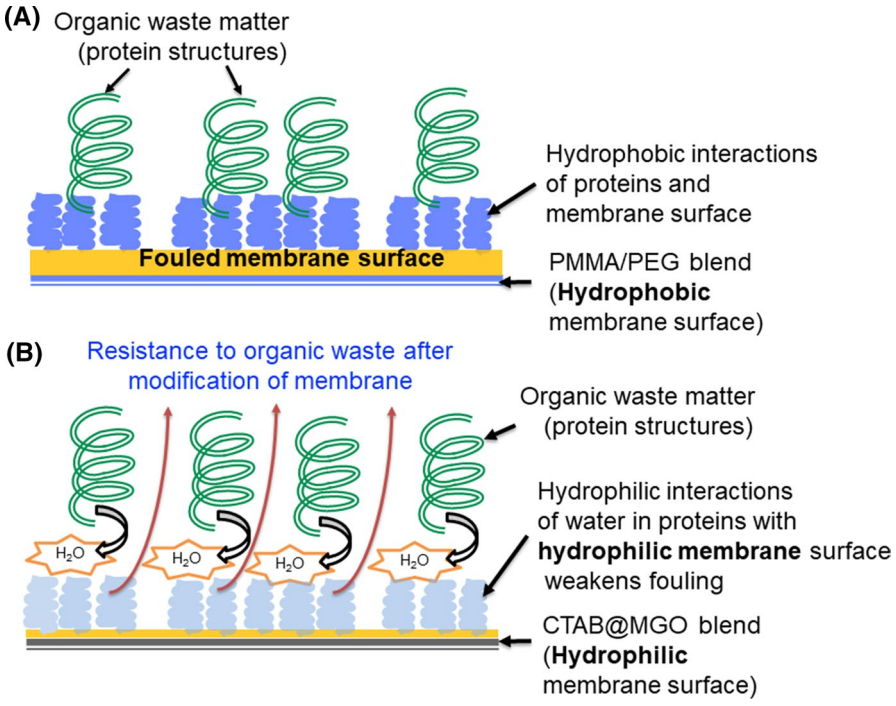

Scheme 2 Mechanism of proteins interaction with the **a** neat and **b** modified blend membranes

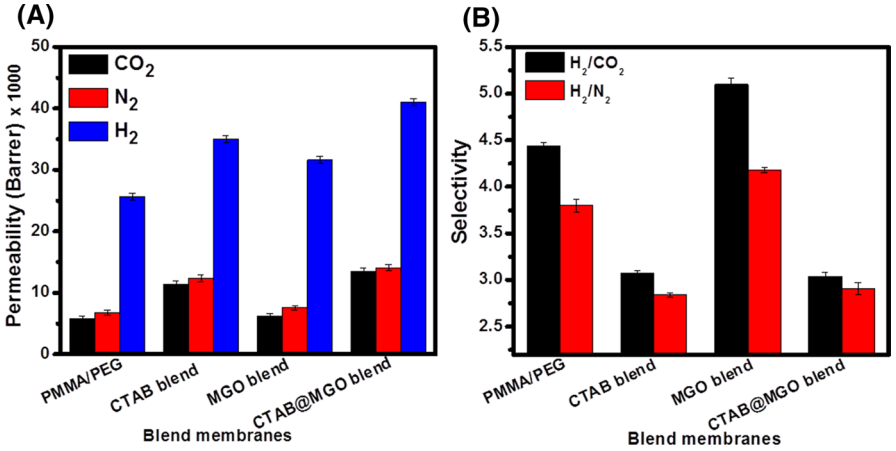

Fig. 6 **a** The gas permeability plots and **b** selectivity for neat, CTAB, MGO and CTAB@MGO blend membranes, respectively

of H_2 (2.89 Å) as compared to nitrogen N_2 (3.64 Å) and CO_2 (3.30 Å) gases. In addition to molecular diameter of gas molecules, permeability across the blend membranes could be affected by different parameters, such as polarity of gases and change in activation energy due to solubility and diffusion process [45]. Here, blend membrane samples showed a relatively low permeability for CO_2 than N_2 gas and this could be associated with its affinity with PEG and increased solubility compared to N_2 (Fig. 6 and Table S2) [35, 46].

The effect of CTAB-immobilized MGO incorporation in PMMA/PEG blend membrane on gas permeability and selectivity is shown in Fig. 6a, b. It is evident that permeability of all the gases across the CTAB@MGO blend membrane is higher as compared to other blend membrane samples (Fig. 6a, b). Incorporation of MGO@CTAB into the blend membrane resulted in increase by two-fold for CO_2 and N_2 and 1.5-fold for H_2 gas permeability as compare to MGO blend membrane. Increase in permeability of CTAB@MGO blend membrane is attributed to CTAB@MGO-directed absorbtion and diffusion of gases in CTAB@MGO blend membrane. In addition, absorption and diffusion of gases might be taking place through diffused crack networks in CTAB@MGO blend as observed in SEM image.

The selectivity of the CTAB@MGO blend membrane for H_2/CO_2 and H_2/N_2 mixtures is shown in Fig. 6b and Table S3. The CTAB@MGO blend membrane showed less selectivity as compared with neat and MGO blend membranes. The decrease in selectivity of CTAB@MGO blend membrane may be associated with less availability of MGO surface due to its coverage with CTAB. This suggests that CTAB@MGO blend membrane is an efficient candidate for permeability of selected gases (H_2, N_2 and CO_2), whereas MGO blend membrane was found to be selective for hydrogen gas separation.

Stability of CTAB in blend membrane

CTAB stability of the prepared blend membranes was determined by gravimetric method. CTAB blend and MGO@CTAB blend (1 cm^2 area) membranes were dipped in de-ionized water for 48 h. The differences in weight of membranes were measured after every 12 h. Initially, CTAB release rate in CTAB blend was found to be 650 ± 50 $\mu g/cm^2$ for 24 h, while in case of CTAB@MGO blend, it was decreased up to 390 ± 60 $\mu g/cm^2$ (Fig. S5). CTAB@MGO blend showed slow release of CTAB with time as compared with CTAB blend. Thus, CTAB@MGO blend enables the minimum negative/toxic effects induced by CTAB release into operational environment. These findings indicated that the prepared modified blend membrane has efficiency in long-term operation and possibly exhibit less toxic with the release of CTAB into the water and other biological environment.

Conclusions

In this study, we demonstrated a facile method to enhance antibacterial and antifouling activity and gas permeation ability of the PMMA/PEG blend membranes incorporated with quaternary ammonium compound immobilized metallic graphene oxide. The CTAB@MGO blend membrane showed 2.5-fold enhanced antibacterial performance by inhibiting bacterial cell growth as compared to MGO blend without CTAB. The CTAB immobilization on MGO showed less protein adsorption on the blend membrane. Thus, CTAB@MGO membrane proved to be an excellent antibacterial and antifouling property that can significantly improve cost-effectiveness as compared with other sophisticated methods for preparing antibacterial and antifouling polymeric membranes. In addition, the CTAB immobilization on MGO played a crucial role in gas permeation and resulted in permeability increase by two- and 1.5-fold gas for (CO_2 and N_2) and H_2, respectively, as compared to control membrane. Gas permeation results demonstrated that CTAB@MGO blend membrane is an efficient candidate for permeability of selected gases (H_2, N_2 and CO_2), whereas MGO blend membrane was found to be selective for hydrogen gas separation. These results highlighted the potential of incorporation of CTAB-immobilized metallic carbon materials into polymeric blend membranes as an effective method to fabricate antibacterial, antifouling and gas permeability membranes for environmental applications.

Acknowledgements The authors thank Dr. Kamlendra Awasthi for gas permeation characterization of samples. We thank Dr. S Bharadwaj and Ashish Pandey for their assistance in sample preparation and SEM imaging of samples.

References

1. Dong L et al (2016) Enhanced CO_2 separation performance of P (PEGMA-co-DEAEMA-co-MMA) copolymer membrane through the synergistic effect of EO groups and amino groups. RSC Adv 6(65):59946–59955
2. Das S, Banthia A, Adhikari B (2006) Removal of chlorinated volatile organic contaminants from water by pervaporation using a novel polyurethane urea–poly (methyl methacrylate) interpenetrating network membrane. Chem Eng Sci 61(19):6454–6467
3. Álvarez-Paino M, Muñoz-Bonilla A, Fernández-García M (2017) Antimicrobial polymers in the nano-world. Nanomaterials 7(2):48
4. Munoz-Bonilla A, Fernández-García M (2012) Polymeric materials with antimicrobial activity. Prog Polym Sci 37(2):281–339
5. Munoz-Bonilla A, Fernandez-Garcia M (2015) The roadmap of antimicrobial polymeric materials in macromolecular nanotechnology. Eur Polym J 65:46–62
6. Sarı A et al (2010) Poly (ethylene glycol)/poly (methyl methacrylate) blends as novel form-stable phase-change materials for thermal energy storage. J Appl Polym Sci 116(2):929–933
7. Silvestre C, Duraccio D, Cimmino S (2011) Food packaging based on polymer nanomaterials. Prog Polym Sci 36(12):1766–1782
8. Bi H et al (2006) Deposition of PEG onto PMMA microchannel surface to minimize nonspecific adsorption. Lab Chip 6(6):769–775
9. Landis RF et al (2016) Cross-linked polymer-stabilized nanocomposites for the treatment of bacterial biofilms. ACS Nano 11(1):946–952
10. Yu W et al (2014) Pre-treatment for ultrafiltration: effect of pre-chlorination on membrane fouling. Sci Rep 4:6513
11. Helin H et al (2008) Anti-fouling ultrafiltration membrane prepared from polysulfone-graft-methyl acrylate copolymers by UV-induced grafting method. J Environ Sci 20(5):565–570
12. Liu Y et al (2016) Enhanced membrane antifouling and separation performance by manipulating phase separation and surface segregation behaviors through incorporating versatile modifier. J Membr Sci 499:406–417
13. Huang X et al (2016) Low-fouling antibacterial reverse osmosis membranes via surface grafting of graphene oxide. ACS Appl Mater Interfaces 8(23):14334–14338
14. Sharma M, Madras G, Bose S (2015) Unique nanoporous antibacterial membranes derived through crystallization induced phase separation in PVDF/PMMA blends. J Mater Chem A 3(11):5991–6003
15. Fang L-F et al (2017) Structures and antifouling properties of polyvinyl chloride/poly (methyl methacrylate)-graft-poly (ethylene glycol) blend membranes formed in different coagulation media. J Membr Sci 524:235–244
16. Hwangbo K-H, Kim Y-J, Cho KY (2012) Fabrication of protein-resistant blend based on PVDF-HFP and amphiphilic brush copolymer made from PMMA and PEGMA. Appl Surf Sci 263:291–296
17. Zhang R et al (2016) Antifouling membranes for sustainable water purification: strategies and mechanisms. Chem Soc Rev 45(21):5888–5924
18. Ma X-Y, Zhang W-D (2009) Effects of flower-like ZnO nanowhiskers on the mechanical, thermal and antibacterial properties of waterborne polyurethane. Polym Degrad Stab 94(7):1103–1109
19. Patricio P et al (2006) Effect of blend composition on microstructure, morphology, and gas permeability in PU/PMMA blends. J Membr Sci 271(1–2):177–185
20. Hong R, Chen Q (2014) Dispersion of inorganic nanoparticles in polymer matrices: challenges and solutions. In: Kalia S, Haldorai Y (eds) Organic–inorganic hybrid nanomaterials, vol 267. Springer, Cham, pp 1–38
21. Hanemann T, Szabó DV (2010) Polymer-nanoparticle composites: from synthesis to modern applications. Materials 3(6):3468–3517
22. Li Y et al (2013) Crystallization of poly (ethylene glycol) in poly (methyl methacrylate) networks. Mater Sci 19(2):147–151
23. Matai I et al (2014) Antibacterial activity and mechanism of Ag–ZnO nanocomposite on *S. aureus* and GFP-expressing antibiotic resistant *E. coli*. Colloids Surf B 115:359–367
24. Bharadwaj S et al (2018) Graphene nano-mesh-Ag-ZnO hybrid paper for sensitive SERS sensing and self-cleaning of organic pollutants. Chem Eng J 336:445–455
25. Ravichandran K et al (2016) Realizing cost-effective ZnO: Sr nanoparticles@ graphene nanospreads for improved photocatalytic and antibacterial activities. RSC Adv 6(72):67575–67585

26. Kavinkumar T, Manivannan S (2016) Uniform decoration of silver nanoparticle on exfoliated graphene oxide sheets and its ammonia gas detection. Ceram Int 42(1):1769–1776
27. Upadhyay RK, Soin N, Roy SS (2014) Role of graphene/metal oxide composites as photocatalysts, adsorbents and disinfectants in water treatment: a review. RSC Adv 4(8):3823–3851
28. Fu Y-J et al (2006) Zeolite-filled PMMA composite membranes: influence of surfactant addition on gas separation properties. Desalination 200(1–3):250–252
29. Mallakpour S, Jarang N (2018) Production of bionanocomposites based on poly (vinyl pyrrolidone) using modified TiO_2 nanoparticles with citric acid and ascorbic acid and study of their physicochemical properties. Polym Bull 75(4):1441–1456
30. Zhang X et al (2017) Membrane biofouling control using polyvinylidene fluoride membrane blended with quaternary ammonium compound assembled on carbon material. J Membr Sci 539:229–237
31. He M et al (2016) Zwitterionic materials for antifouling membrane surface construction. Acta Biomater 40:142–152
32. Olkowska E, Polkowska Z, Namiesnik J (2011) Analytics of surfactants in the environment: problems and challenges. Chem Rev 111(9):5667–5700
33. Tüzüner Ş, Demir MM (2015) Dispersion of organophilic Ag nanoparticles in PS-PMMA blends. Mater Chem Phys 162:692–699
34. Rana D, Matsuura T (2010) Surface modifications for antifouling membranes. Chem Rev 110(4):2448–2471
35. Kumar R, Kumar M, Awasthi K (2016) Functionalized Pd-decorated and aligned MWCNTs in polycarbonate as a selective membrane for hydrogen separation. Int J Hydrog Energy 41(48):23057–23066
36. Upadhyay S, Bagheri S, Hamid SBA (2014) Enhanced photoelectrochemical response of reduced-graphene oxide/$Zn1-xAgxO$ nanocomposite in visible-light region. Int J Hydrog Energy 39(21):11027–11034
37. Yoo D-H et al (2012) Photocatalytic performance of a Ag/ZnO/CCG multidimensional heterostructure prepared by a solution-based method. J Phys Chem C 116(12):7180–7184
38. Meng W et al (2015) Structure and interaction of graphene oxide–cetyltrimethylammonium bromide complexation. J Phys Chem C 119(36):21135–21140
39. Liu Q et al (2017) Enhanced mechanical and thermal properties of CTAB-functionalized graphene oxide–polyphenylene sulfide composites. High Perform Polym 29(8):889–898
40. Zhang Z, Lin M (2014) Fast loading of PEG–SH on CTAB-protected gold nanorods. RSC Adv 4(34):17760–17767
41. Shinzawa H, Mizukado J, Kazarian SG (2017) Fourier transform infrared (FT-IR) spectroscopic imaging analysis of partially miscible PMMA–PEG blends using two-dimensional disrelation mapping. Appl Spectrosc 71(6):1189–1197
42. Singh A, Chandra A (2013) Graphene and graphite oxide based composites for application in energy systems. Phys Status Solidi (b) 250(8):1483–1487
43. Thomas K et al (2008) Raman spectra of polymethyl methacrylate optical fibres excited by a 532 nm diode pumped solid state laser. J Opt A Pure Appl Opt 10(5):055303
44. Putz KW et al (2010) High-nanofiller-content graphene oxide–polymer nanocomposites via vacuum-assisted self-assembly. Adv Funct Mater 20(19):3322–3329
45. Barrer R, Rideal EK (1939) Permeation, diffusion and solution of gases in organic polymers. Trans Faraday Soc 35:628–643
46. Gacal BN, Filiz V, Abetz V (2016) The synthesis of poly (ethylene glycol)(PEG) containing polymers via step-growth click coupling reaction for CO_2 separation. Macromol Chem Phys 217(5):672–682